I&EC research
Industrial & Engineering Chemistry Research

Article

pubs.acs.org/IECR

Optimization of in Situ Gasification Chemical Looping Combustion through Experimental Investigations with a Cold Experimental System

Xiaojia Wang,[†,‡] Baosheng Jin,[*,†] Hao Liu,[*,‡] Wei Wang,[†] Xianli Liu,[†] and Yong Zhang[†]

[†]Key Laboratory of Energy Thermal Conversion and Control of Ministry of Education, School of Energy & Environment, Southeast University, Nanjing 210096, People's Republic of China

[‡]Faculty of Engineering, University of Nottingham, Nottingham NG7 2RD, U.K.

ABSTRACT: In situ gasification chemical looping combustion (iG-CLC) is a promising coal combustion technology for implementing CO_2 capture with a low energy penalty. A novel iG-CLC cold experimental system was developed in the authors' previous work (*Ind. Eng. Chem. Res.* **2013**, *52*, 14208). It mainly consists of a high-flux circulating fluidized bed (HFCFB) riser as the fuel reactor and a cross-flow moving bed as the air reactor. As an extension of that work, in this study, we further optimized the iG-CLC system by redesignung the air reactor to enhance the carrying capacity of the gas flow and developing a two-stage separation system by adding a second-stage cyclone to the original first-stage inertial separator. Stability in operation and flexibility in adjusting operating parameters were achieved with the improved system. In the riser (fuel reactor), higher solids fluxes and solids holdups were achieved, which should enhance the gas−solid contact and promote the complicated heterogeneous reactions. In the moving bed (air reactor), the carrying capacity of the gas flow was significantly enhanced, which should lead to a great increase in the system power capacity. The confirmation of the ability to control the gas flow directions in the two reactors means that the gas bypassing between the two reactors can be restrained so as to ensure a high CO_2 concentration in the exhaust of the fuel reactor. The high global separation efficiency and selective separation efficiency of the new two-stage separation system for fine particles indicate that a high combustion efficiency of coal can be achieved with a hot iG-CLC system.

1. INTRODUCTION

Chemical looping combustion (CLC), which combines fuel combustion and CO_2 sequestration in situ, is regarded as a promising combustion technology with a low cost of CO_2 separation.[1,2] Previous studies on CLC process mainly focused on gaseous fuels.[3−5] Recently, because of the more abundant reserves and lower price of coal with respect to gaseous fuels, coal-fired CLC has attracted increasing attention.[6−10] One of the promising applications of coal-fired CLC is so-called in situ gasification chemical looping combustion (iG-CLC), which integrates coal gasification and subsequent reduction of the oxygen carrier in the fuel reactor.[11−13]

During the iG-CLC process, the deactivation of the oxygen carrier (OC) is inevitable because of the presence of organic sulfur in the coal. Moreover, the particles of the OC can be lost as agglomerates formed with the coal ash. Therefore, compared with the gas-fueled CLC, iG-CLC technology must face the serious issue of a much larger mass loss of the OC. In this context, the use of low-cost materials such as natural minerals as oxygen carriers has attracted great interest.[10,14−19]

This study proposes a novel iG-CLC system with a low-grade iron ore as the oxygen carrier (OC), as shown in Figure 1. A high-flux circulating fluidized bed (HFCFB) riser is employed as the fuel reactor (FR) because it can provide favorable gas−solid contact and sufficient solids holdups over the whole reactor height.[15,20−24] A cross-flow moving bed is employed as the air reactor (AR) because of its advantages in terms of low pressure drop, steady solids flow, and compact structure,[15,25−27] which can be simply placed in the middle of the CFB downcomer. Meanwhile, a specific two-stage separation system is designed to achieve selective separations of the large OC particles and fine combustible particles (i.e., char and carbonaceous coal ash). The first-stage separator is a low-efficiency inertial separator where most of the particles (mainly the OC) are separated to the AR for regeneration. The second-stage separator is a high-efficiency cyclone where most of the fine combustible particles are separated and recirculated to the fuel reactor for further reactions. The combination of a low-resistance inertial separator and a high-resistance cyclone can ensure a low pressure drop over the whole separation system under high-flux conditions.

In our previous study, we successfully built a first-generation iG-CLC cold experimental system.[15] After a series of tests, the steady operation of the whole system under conditions of high solids flux was realized, verifying the feasibility of the apparatus. Then, the control of the gas flow directions in the two reactors was also achieved, which could restrain the gas bypassing between the two reactors so as to ensure a high CO_2 concentration in the exhaust of the fuel reactor. Moreover, flexible adjustments of the operating parameters (e.g., solids holdups and gas−solid residence time) were implemented, which could help a real iG-CLC system achieve a higher CO_2 concentration and fuel conversion in the operating process.

Received: February 3, 2015
Revised: May 6, 2015
Accepted: May 12, 2015
Published: May 12, 2015

DOI: 10.1021/acs.iecr.5b00471
Ind. Eng. Chem. Res. 2015, 54, 5749−5758

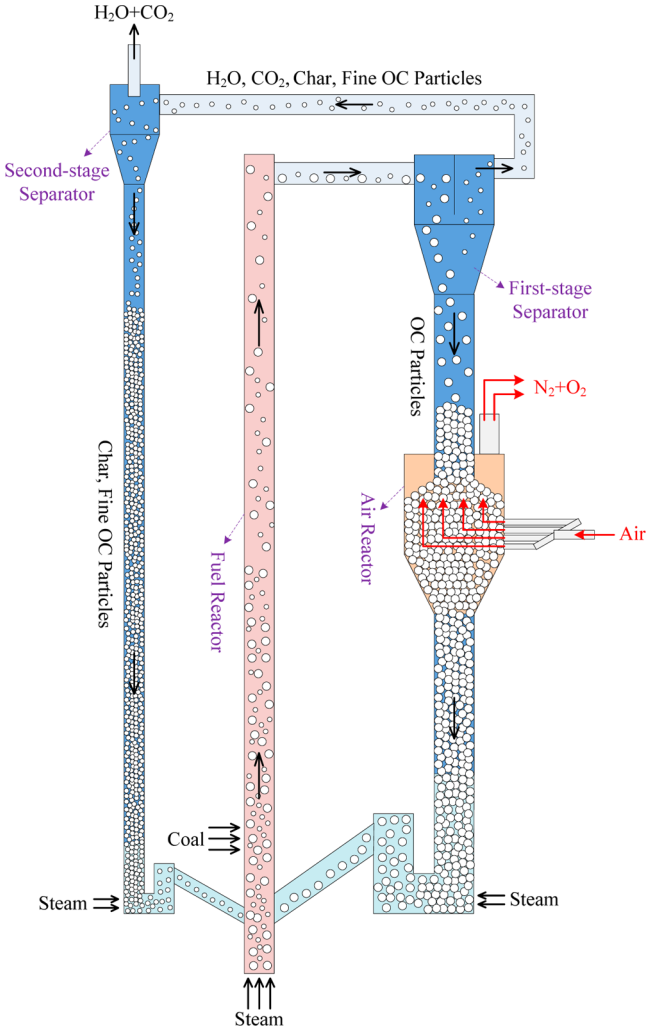

Figure 1. Schematic diagram of the proposed iG-CLC system.

However, this first-generation cold experimental system still has limitations in terms of particle separation and combustion capacity. First, its separation system consisted of only a single inertial separator. Thus, it was impossible to study the selective separation performance of the separation system on large OC particles and fine combustible particles, which is very important for the combustion efficiency of coal. Meanwhile, the originally designed cross-flow moving bed (i.e., AR) had a small gas-flow carrying capacity and thus required a large cross-sectional area, which would limit the proposed novel iG-CLC system to applications in small-scale power plants.

With the aim of overcoming these limitations, we carried out a series of improvements to the first-generation cold experimental system with the addition of a second-stage cyclone separator and the optimization of the cross-flow moving bed (i.e., AR). In the present study, the experimental investigation consisted of the following four parts: (1) In the baseline experiment, the purpose was to establish stable operation and implement flexible adjustments of operating parameters in the improved system. The addition of the second-stage separator changed the particle circulation from single loop to double loop and made the operation of the improved system much more complex than that of the first-generation system. (2) Tracer experiments were then performed to investigate the gas flow directions of the two reactors under different pressure ratios (P_b/P_a) using the method of gas tracing. At a suitable value of P_b/P_a, the gas bypassing between the two reactors can be restrained so as to ensure a high CO_2 concentration in the exhaust of the fuel reactor and a high capture efficiency of CO_2. (3) The feasibility test of the improved cross-flow moving bed focused on an investigation of the flow characteristics in the improved cross-flow moving bed, especially the increase in the gas-flow carrying capacity, which can contribute significantly to an increase in system thermal power. (4) Finally, separation performance experiments were performed to investigate the global separation efficiency and selective separation efficiency of the two-stage separation system for fine particles, which is very important for the combustion efficiency of coal.

2. EXPERIMENTAL SECTION

2.1. Materials. The oxygen carrier selected in this study was a low-grade iron ore from Harbin, China. Prior to the experiments, the iron ore particles were crushed and sieved to a mean diameter of 0.65 mm. The apparent density of the iron ore was 2558 kg/m^3, and the bulk density was 1535 kg/m^3. The minimum fluidization gas velocity of the iron ore under the cold experimental conditions (U_{min}) was measured to be 0.30 m/s by means of a small bubbling fluidized bed (0.12 m length × 0.04 m width × 1.0 m height).

The coal used was a Shenhua bituminous coal from the Inner Mongolia Autonomous Region of China, which was sieved to a fine mean diameter of 0.1 mm. The apparent and bulk densities of this coal were 1270 and 744 kg/m^3, respectively.

Most of the cold experiments were carried out using just the iron ore as the bed material. However, to estimate the recirculation efficiency of the fine combustible particles (e.g., char and carbonaceous coal ash) during the iG-CLC process, we especially carried out an investigation of the selective separation performance of the two-stage separation system for fine particles, where the fine coal particles were used to represent the fine combustible particles in hot applications. Prior to this investigation, fine coal particles were premixed with the larger iron ore particles at a preselected proportion.

2.2. Improved Cold Experimental Setup. Figure 2 schematically shows the improved cold experimental setup of the proposed iG-CLC system. Here, only a brief introduction of the experimental system is provided, mainly focusing on the improved (new) parts. A more detailed description can be found in our previous study on the first-generation system.[15]

This cold iG-CLC system mainly consists of a vertical riser (0.06 m i.d. × 5.8 m height) (6), a first-stage inertial separator (8), a first-stage downcomer (0.1 m i.d. × 1.7 m height above the air reactor and 0.1 m length × 0.1 m width × 2.0 m height below the air reactor) (9), an improved cross-flow moving-bed air reactor (11), a first-stage J valve (14), a feeder (15), a second-stage cyclone separator (16), a second-stage downcomer (0.05 m i.d. × 5 m height) (17), a second-stage J valve (18), and a bag filter (19). Some sections of the riser and the two-stage downcomers are made of plexiglas so as to allow visualization. The air stream from a 90 kW air compressor (26) was fed into the HFCFB riser (i.e., FR) through a gas distributor. Another air stream from an 18 kW air compressor (27) was fed into the cross-flow moving bed (i.e., AR) through a tube distributor.

Figure 3 shows a detailed schematic drawing of the improved cross-flow moving-bed air reactor (11). It mainly consists of a particle inlet, a particle outlet, a gas inlet, a gas outlet, a tube

DOI: 10.1021/acs.iecr.5b00471
Ind. Eng. Chem. Res. 2015, 54, 5749−5758

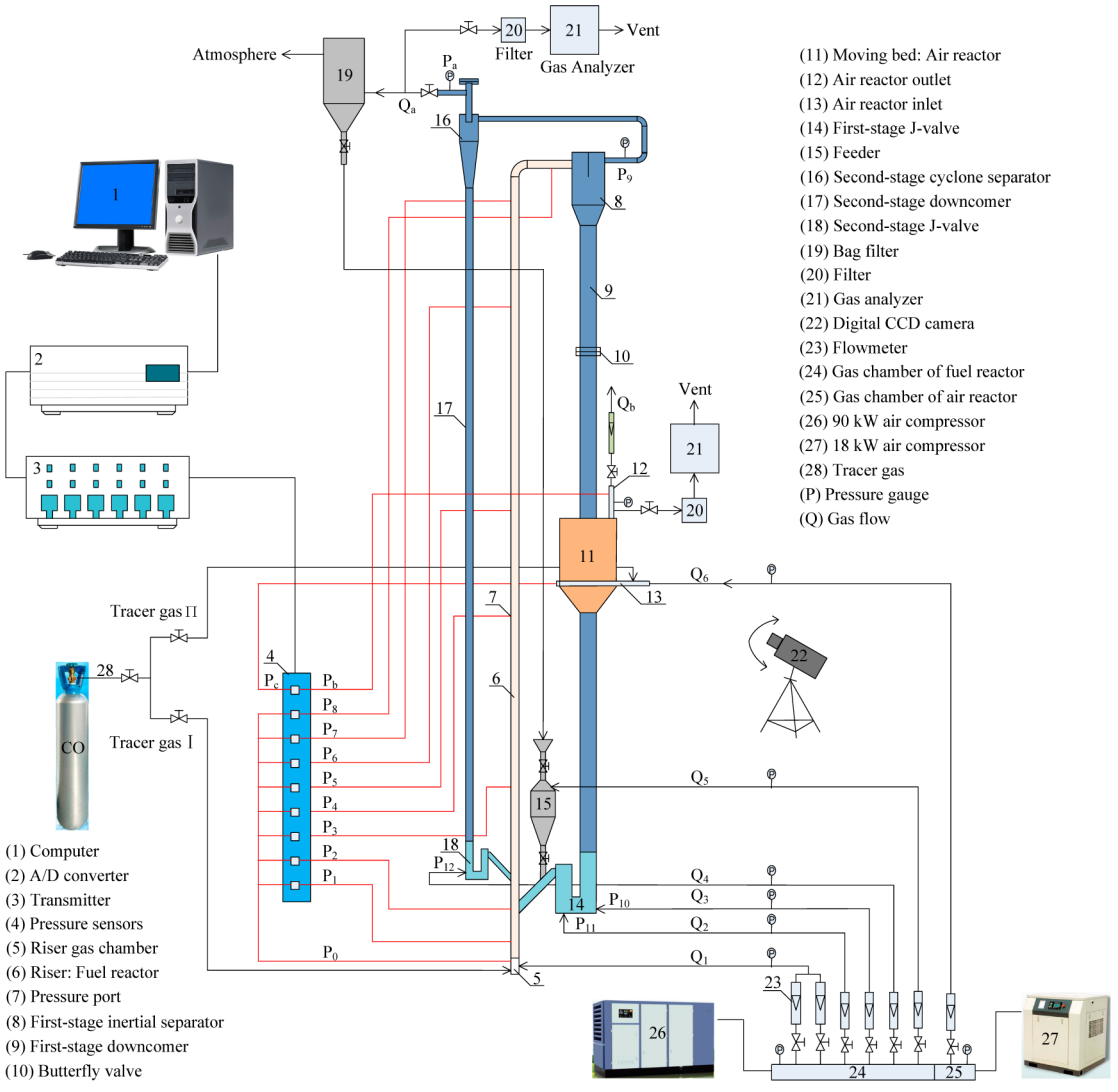

Figure 2. Schematic diagram of the improved cold experimental setup for the proposed iG-CLC system.

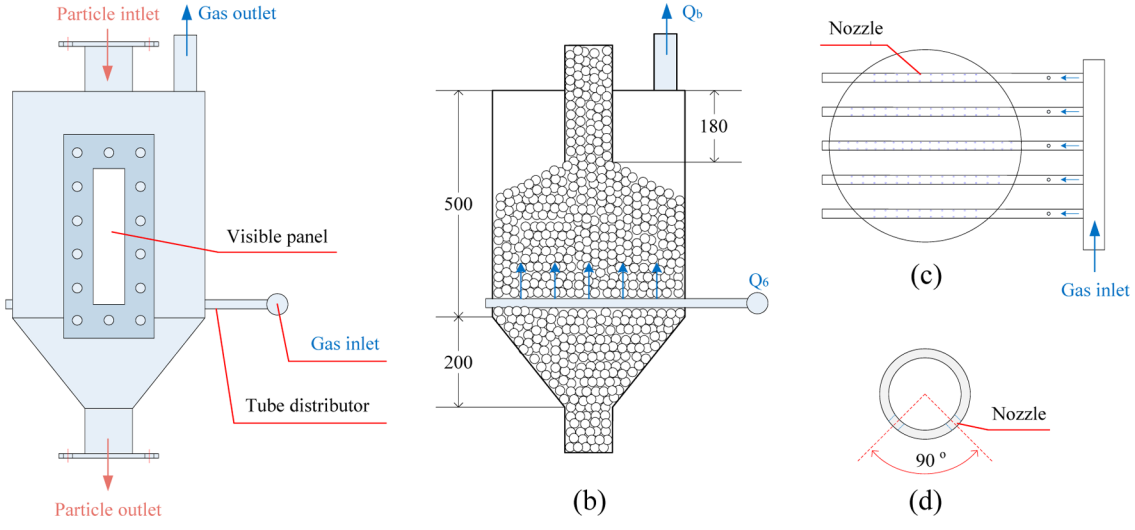

Figure 3. Schematic drawing of the improved cross-flow moving-bed air reactor: (a) front view, (b) inside view, (c) top view of the tube distributor, (d) side view of one tube of the distributor.

distributor, a cylindrical channel, a cone channel, and a visible panel. The cylindrical channel is 0.5 m in height and 0.418 m in inner diameter, and the cone channel is 0.2 m in height. From Figure 3b, one can observe that the particle inlet tube was

DOI: 10.1021/acs.iecr.5b00471
Ind. Eng. Chem. Res. 2015, 54, 5749−5758

designed to be inserted into the cylindrical channel at a depth of 0.18 m. Thus, an even buffer zone was formed for the exhaust stream before it entered the asymmetric gas outlet, which should be beneficial for the pressure and gas flow distributions in the air reactor. As shown in Figure 3c,d, the tube distributor was made up of five parallel horizontal tubes. Each tube contained 20−40 nozzles are arranged symmetrically at the bottom of the tube with an angle of 90°. During system operation, the particles moved down from the upper particle inlet, whereas the gas stream flowed upward from the lower nozzles of the tube distributor. Thus, a cross-flow between the gas and solids phases formed, which is good for the gas−solid contact and reaction.

The gas flow rates were controlled and measured by calibrated rotameters. The pressures were measured by pressure manometers and adjusted by back-pressure regulators. The pressure drops were measured by a multichannel differential pressure transducer, and the related data were continuously logged on a computer. All gas flow rates with the subscript "sta" in this article were normalized to the standard state (101.325 kPa for pressure and 273.15 K for temperature). CO with a high purity (99.99%) was selected as the tracer gas (28).

2.3. Experimental Procedures. *2.3.1. Baseline Experiment.* Prior to the baseline experiment, the particles of iron ore were packed in the two-stage downcomers. The initial packing heights were about 4 m in the first-stage downcomer (i.e., about 0.7 m above the top of the air reactor) and about 3 m in the second-stage downcomer. At the beginning of the experiment, the gas stream from the 90 kW air compressor was injected into the fuel reactor from the two-stage J valves and the riser distributor so as to drive the particles into circulation. When the particle circulation became stable, another gas stream from the 18 kW air compressor was injected into the moving-bed air reactor and matched into the original circulation system. Finally, through a series of fine adjustments to the operating parameters (e.g., gas inlet flow rates of the two reactors and solids flux), the whole system could reach an ideal balance with the desired operating conditions.

2.3.2. Tracer Experiment. As the gas−solid flow in the whole system became stable, tracer gas I was injected into the riser (FR). One minute later, gas sampling began at the outlets of the second-stage cyclone separator and the cross-flow moving bed (AR). After the gas sampling, tracer gas I was discontinued, and tracer gas II was injected into the inlet of the moving bed (AR). Then, similar gas sampling was carried out 1 min later. The measurements of the components of the sampled gases together with the gas flow rates in the two reactors were used to characterize the gas flow directions of the two reactors. A detailed explanation of the data processing can be found in section 2.4.3.

2.3.3. Feasibility Test of the Improved Cross-Flow Moving Bed. As the gas stream from the 90 kW air compressor was injected into the fuel reactor and the particle circulation became stable, another gas stream from the 18 kW air compressor was injected into the moving-bed air reactor with an increasing gas flow rate. During the process of increasing the gas flow rate, the gas−solid flow state in the air reactor was monitored in real time. When the flow behaviors were observed to become unstable from the previous continuous steady state, the maximum fluidizing number, $N_{a,max}$, was determined.

Furthermore, as the whole system was adjusted to be stable, the effect of a certain operating parameter (e.g., fluidizing number N_a, solids flux G_s, and pressure ratio P_b/P_a) on the pressure drop of the moving bed could be investigated by adjusting the variable parameter while keeping all other parameters constant.

2.3.4. Separation Performance Experiment. Initially, the fine coal particles were premixed with the iron ore particles at a preselected proportion and packed together in the first-stage downcomer. However, the bed material packed in the second-stage downcomer was only the iron ore. At the beginning of the experiment, the gas stream was injected into the fuel reactor from the first-stage J valve and the riser distributor to drive the particles into circulation. It should be noted that, because of the closure of the second-stage J valve, there was only the input of particle flow but without the output in the second-stage downcomer when the particle circulation began.

The output solids mass flow rate of the first-stage downcomer was measured by a butterfly valve located in the upper part of the first-stage downcomer. The rotary blade in the butterfly valve was drilled and covered with a fine wire mesh. As the butterfly valve was closed, the amount of the solids reduced in the lower section below the butterfly valve was recorded for a given time period, from which the output solids mass flow rate was derived.[28] Then, the input solids mass flow rate of the second-stage downcomer was measured by recording the amount of solids increased within a given time period. After the experiment, the mass fraction of coal in the solids mixture collected by the second-stage downcomer could be easily measured by the sieving method according to the difference in particle size between the fine coal particles and the large iron ore particles. With the measurement of these and other parameters, the selective separation efficiency and the global separation efficiency of the two-stage separation system for fine particles of coal were determined. A detailed explanation of the data processing can be found in section 2.4.5.

2.4. Data Evaluation. *2.4.1. Apparent Solids Holdup.* The cross-sectional average solids holdup (ε_s) in the riser can be calculated as[15,28−31]

$$\Delta P_Z/\Delta Z \approx [\rho_s \varepsilon_s + \rho_g(1-\varepsilon_s)]g \quad (1)$$

where ΔP_Z is the local pressure drop at two adjacent riser elevations.

2.4.2. Gas Flow Rates. The total inlet flow rate of the system normalized to the standard state can be calculated as[15]

$$\begin{aligned} Q_{in,sta} &= Q_{1,sta} + Q_{2,sta} + Q_{3,sta} + Q_{4,sta} + Q_{5,sta} + Q_{6,sta} \\ &= Q_{g,sta} + Q_{6,sta} \end{aligned} \quad (2)$$

where $Q_{1,sta}$, $Q_{2,sta}$, $Q_{3,sta}$, $Q_{4,sta}$, $Q_{5,sta}$, and $Q_{6,sta}$ represent the inlet air flow rate of the riser, the fluidizing air flow rate of the first-stage J valve, the aeration air flow rate of the first-stage J valve, the aeration air flow rate of the second-stage J valve, the aeration air flow rate of the feeder, and the inlet air flow rate of the moving bed, respectively. $Q_{g,sta}$ is used to denote the sum of $Q_{1,sta}-Q_{5,sta}$.

The total outlet flow rate of the system normalized to the standard state can be calculated as

$$Q_{out,sta} = Q_{a,sta} + Q_{b,sta} \quad (3)$$

where $Q_{a,sta}$ and $Q_{b,sta}$ represent the outlet air flow rate of the second-stage cyclone separator and the outlet air flow rate of the moving bed, respectively. All of these inlet/outlet flow rates were measured by flow meters except $Q_{a,sta}$, which was

DOI: 10.1021/acs.iecr.5b00471
Ind. Eng. Chem. Res. 2015, 54, 5749−5758

calculated according to the mass balance of air stream between the inlets and outlets as

$$Q_{a,sta} = Q_{out,sta} - Q_{b,sta} = Q_{in,sta} - Q_{b,sta} = Q_{g,sta} + Q_{6,sta} - Q_{b,sta} \quad (4)$$

2.4.3. Tracer Gas. Using tracer gas I, we investigated the distribution of the exhaust gas from the riser (FR) outlet. f_I represents the fraction of the riser exhaust gas bypassing into the air reactor[15]

$$f_I = \frac{Q_{b,sta}x_{b,CO}}{Q_{a,sta}x_{a,CO} + Q_{b,sta}x_{b,CO}} \times 100\% \quad (5)$$

where $x_{a,CO}$ and $x_{b,CO}$ are the concentrations of tracer gas I measured at the outlets of the second-stage cyclone separator and the moving bed (AR), respectively. Thus, $Q_{a,sta}x_{a,CO}$ and $Q_{b,sta}x_{b,CO}$ represent the volume flow rates of tracer gas I at the outlets of the second-stage cyclone separator and the moving bed (AR), respectively.

We also investigated the distribution of the gas from the moving-bed (AR) inlet through the use of tracer gas II. f_{II} represents the fraction of the gas from the moving-bed inlet bypassing into the second-stage cyclone outlet[15]

$$f_{II} = \frac{Q_{a,sta}x'_{a,CO}}{Q_{a,sta}x'_{a,CO} + Q_{b,sta}x'_{b,CO}} \times 100\% \quad (6)$$

where $x'_{a,CO}$ and $x'_{b,CO}$ are the concentrations of tracer gas II measured at the outlets of the second-stage cyclone separator and the moving bed (AR), respectively.

2.4.4. Fluidizing Numbers in the Two Reactors. N_f represents the fluidizing number in the fuel reactor, which is defined as the ratio between the superficial gas velocity of the fuel reactor and the minimum fluidizing velocity of the bed material under the operating conditions of the fuel reactor[15]

$$N_f = \frac{U_f}{U_{min}} \quad (7)$$

where U_f and U_{min} are the superficial gas velocity of the fuel reactor and the minimum fluidizing velocity of the bed material, respectively.

N_a represents the fluidizing number in the air reactor, which is defined as the ratio between the superficial gas velocity of the air reactor and the minimum fluidizing velocity of the bed material[15]

$$N_a = \frac{U_a}{U_{min}} \quad (8)$$

where U_a is the superficial gas velocity of the air reactor (i.e., the ratio between the total gas flow rate in the air reactor and the cross-sectional area).

2.4.5. Separation Efficiencies of the Two-Stage Separation System. η represents the global separation efficiency of the two-stage separation system for fine coal particles, which is defined as the ratio between the mass flow rate of coal separated by the two-stage separation system and the output mass flow rate of coal

$$\eta = \frac{M_1Y_1 + M_2Y_2}{M_0Y_0} = 1 - \frac{M_3Y_3}{M_0Y_0} = 1 - \frac{M_3tY_3}{M_0tY_0} = 1 - \frac{m_3(t)Y_3}{M_0tY_0} \quad (9)$$

where M_0 is the output solids mass flow rate (including OC and coal); M_1, M_2, and M_3 are the solids mass flow rates separated by the first-stage separator, the second-stage separator, and the bag filter, respectively; Y_0, Y_1, Y_2, and Y_3 are the corresponding mass fractions of coal in the solid particles; t is the testing time; and $m_3(t)$ is the mass of solids collected by the bag filter during the testing time.

η_s represents the selective separation efficiency of the two-stage separation system for fine coal particles, which is defined as the ratio between the mass flow rate of coal separated by the second-stage separator and the output mass flow rate of coal

$$\eta_s = \frac{M_2Y_2}{M_0Y_0} \quad (10)$$

During the iG-CLC process with an HFCFB fuel reactor, the unreacted fine combustible particles (including char and carbonaceous coal ash) from the fuel reactor should be sent back for further reaction by circulation so as to achieve a high conversion of fuel. In this respect, the two-stage separation system of the novel iG-CLC system needs to achieve the following two targets: (1) It should have a high global separation efficiency for fine particles (i.e., η) so that the escape of fine combustible particles from the separation system can be minimized. (2) It should also have high selective separation efficiency for fine particles (i.e., η_s) so that most of the unreacted fine combustible particles can be separated into the second-stage downcomer and sent back to the fuel reactor for further CLC reactions and avoid being consumed by the air in the air reactor, which is located in the first-stage downcomer.

3. RESULTS AND DISCUSSION

3.1. Baseline Experiment. During the operating process, the system is controlled and adjusted mainly by the following four process variables: solids flux G_s, pressure ratio between the two reactors P_b/P_a (where P_a and P_b represent the pressures at the outlets of the second-stage cyclone separator and the cross-flow moving bed, respectively), fluidizing number in the fuel reactor N_f, and fluidizing number in the air reactor N_a. Table 1 details how adjustments of these variables can be achieved.

Table 1. Adjustment Measures of the Main Process Variables

variable	adjustment measure
solids mass flux G_s (kg/m^2·s)	regulation of the rotameter of Q_3
pressure ratio P_b/P_a	regulation of the valve at the outlet of AR to change the value of P_b
fluidizing number in the fuel reactor N_f	regulation of the rotameter of Q_1
fluidizing number in the air reactor N_a	regulation of the rotameter of Q_6

To facilitate the analysis, the operating conditions of G_s = 400 kg/m^2·s, P_b/P_a = 2.5, N_f = 27, and N_a = 0.28 are defined as the reference conditions for the improved system. Compared with the previous study on the first-generation system,[15] a higher solids mass flux was achieved in this study, which is beneficial for increasing the solids holdup in the riser.

DOI: 10.1021/acs.iecr.5b00471
Ind. Eng. Chem. Res. 2015, 54, 5749−5758

3.1.1. Stability of the Improved System. Figure 4 shows the whole-system pressure profiles of the improved iG-CLC cold

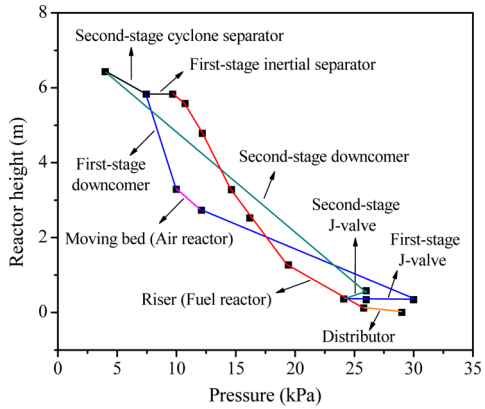

Figure 4. Whole-system pressure profiles of the improved apparatus under the reference conditions.

experimental system under the reference conditions. It can be observed that the pressure fields of the whole system are smoothly connected with each other, indicating the stability of system and the good matching between components.

The system pressure drops under this set of conditions, owing to the much higher solids mass flux, were generally higher than those under the previous reference conditions for the first-generation system.[15] The pressure drops in the riser (FR) and the two-stage separation system were 16.1 and 5.7 kPa, respectively, higher than the corresponding values (8.4 and 3.6 kPa) for the first-generation system under the previous reference conditions, which could achieve a solids flux of only 220 kg/m^2·s. The pressure drop between the inlet and outlet of the improved cross-flow moving bed (AR) was only 2.0 kPa under a fluidizing number of N_a = 0.28. Considering that the pressure drop of the first-generation AR reached 0.778 kPa under a much lower fluidizing number (N_a = 0.042), the advantage of the moving bed in terms of low pressure drop is retained.

3.1.2. High Solids Holdup in the Riser. Figure 5 shows the axial profile of the apparent solids holdup along the CFB riser (FR). It can be observed that the solids holdup generally decreased along the bed height, which is consistent with the

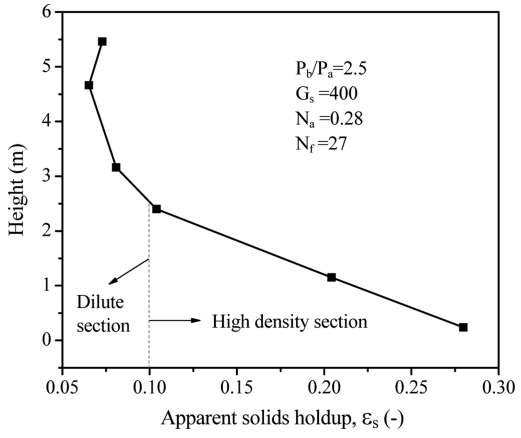

Figure 5. Axial profile of the apparent solids holdup along the riser (reference conditions).

previous observations for the first-generation system.[15] However, the difference is that the much higher solids mass flux (G_s = 400 kg/m^2·s) achieved in this study led to higher solids holdups in the riser. Thus, the height of the high-density flow region ($\varepsilon_s \geq 0.1$)[15,28] was obviously increased, reaching almost half of the riser height. Meanwhile, the solids holdups in the dilute section were higher than 0.05, indicating that the flow structure in the riser under the new reference conditions was very close to the full high-density structure.

3.2. Tracer Experiment. As mentioned in the earlier work,[15] the restraint of N_2 from the air reactor bypassing into the exhaust gas of the fuel reactor so as to ensure a high CO_2 concentration is one of the key requirements for CLC. Therefore, f_{II} should be equal to or approach zero. In addition, although f_I does not affect the concentration of CO_2 in the exhaust of the fuel reactor, the smaller the value of f_I, the higher the CO_2 capture efficiency that can be achieved.

Table 2 lists the parameters required for the calculations of f_I and f_{II} under the reference conditions, according to eqs 4−6. It

Table 2. Parameters Measured in the Tracer Experiment (Reference Conditions)

parameter	units	value	parameter	units	value
P_b/P_a	−	2.5	$x_{b,CO}$	ppm	3
$Q_{g,sta}$	m^3/h	105	$x'_{a,CO}$	ppm	0
$Q_{6,sta}$	m^3/h	38	$x'_{b,CO}$	ppm	1214
$Q_{b,sta}$	m^3/h	46	f_I	%	0.23
$x_{a,CO}$	ppm	630	f_{II}	%	0

can be seen that the value of f_{II} is 0, indicating that N_2 bypassing has been completely restrained and, hence, that a high CO_2 concentration can be assured. Meanwhile, f_I was also limited to a very small value (0.23%), indicating a high capture efficiency of CO_2.

3.3. Feasibility Test of the Improved Cross-Flow Moving Bed. *3.3.1. Improvement in the Carrying Capacity of the Gas Flow.* One of the main disadvantages of the first-generation cold iG-CLC system was the small carrying capacity of the gas flow in the cross-flow moving bed (AR), meaning that a large cross-sectional area was required for a given gas flow rate. However, as the cross-sectional area of the moving bed in the first-generation system was related to the downcomer height, which would be fixed in utility boilers, increasing the cross-sectional area would be very limited. Thus, according to our previous assessment, the proposed iG-CLC system with the first-generation cross-flow moving-bed air reactor could be applied only to small boilers (e.g., 50 $MW_{thermal}$) with low air flow rates so as to keep the cross-sectional area of the air reactor within a practical range.[15] Hence, increasing the carrying capacity of the gas flow in the air reactor is a key factor in increasing the thermal power of the proposed iG-CLC system.

With the new design, the original horizontal gas flow in the moving bed is changed to vertical upflow, so that the falling particles in the improved moving bed receive vertical upward flotage from the gas flow instead of a horizontal pushing force. Obviously, the falling particles are more resistant to the flotage because of gravity, and this provides the rationale for our improvement to the moving-bed air reactor. Moreover, with the orderly distribution of a large number of nozzles, uniform inlet air flow in the air reactor was also achieved. Thus, local high gas

DOI: 10.1021/acs.iecr.5b00471
Ind. Eng. Chem. Res. 2015, 54, 5749−5758

velocities and uneven pressure distributions can be largely avoided so as to ensure the stability of the particle flow.

As shown in Figure 6, an obvious increase in the maximum fluidizing number of the air reactor $N_{a,max}$ was achieved, from

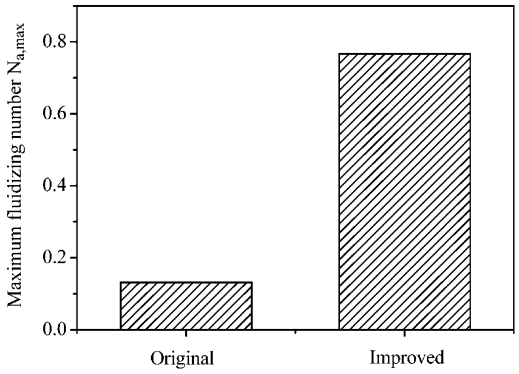

Figure 6. Comparison of the maximum fluidizing number in the air reactor, $N_{a,max}$, before and after improvement.

0.132 for the first-generation system to 0.766 for the present improved system. This indicates that the improved air reactor can make the proposed iG-CLC system suitable for larger power plants, from the original 50 $MW_{thermal}$ to about 300 $MW_{thermal}$ with the same cross-sectional area.

Better still, the cross-sectional area of the improved moving bed is related to only the reactor diameter instead of height. Thus, it should be feasible to connect several air reactors in series in the vertical direction so as to achieve staged OC regeneration, that is, some of the recirculating OC particles being treated in each air reactor. With this method, the total air flow rate and, further, the power capacity of the proposed iG-CLC system can be significantly increased to meet the high power requirements of future utility boilers.

Here, it is necessary to explain how the maximum fluidizing number, $N_{a,max}$, was determined from the experiments. When the gas flow rate in the air reactor was gradually increased from a small value, we observed that the gas−solid flow remained steady until the gas flow reached a certain value when the flow behaviors began to become unstable: (1) Some bubbles were generated in some local regions of the air reactor. (2) Some particles were entrained out of the air reactor. (3) The downward flow of particles sped up significantly because of the effect of loosening them from the bubbles. In a practical iG-CLC application, these unstable flow behaviors will cause a series of negative effects. First, a proportion of air will pass the air reactor through the bubble phase. Thus, the gas−solid contact efficiency will be weakened, and some air will be unnecessarily wasted (i.e., without reacting with the OC). Second, the continuing loss of particles through entrainment will gradually destroy the system balance and stability. Admittedly, this issue can be solved by adding separation and recirculation equipment at the outlet of the air reactor to return the OC particles. However, such a measure would greatly increase the system complexity and cost. Finally, the acceleration of downward particle flow will lead to a reduction in the particle residence time in the air reactor, which will lower the regeneration degree of the oxygen carrier. To avoid these negative effects on the flow and reaction performances, we define the fluidizing number when the unsteady gas−solid flow in the air reactor begins to appear as the maximum fluidizing number, $N_{a,max}$. In a practical iG-CLC system, the fluidizing number of the air reactor should be lower than $N_{a,max}$ to avoid instability and other negative effects in the air reactor.

3.3.2. Effects of Operating Conditions. In practical iG-CLC applications, the visualization of the particle flows is usually impossible because of high operating temperatures and/or pressures, and hence, the particle flow characteristics in the air reactor can be judged only by the measurement and analysis of the pressure drops. Therefore, investigations of the relationships between the pressure drops and their influencing factors are significant in terms of understanding the real-time gas−solid flow characteristics in the air reactor and selecting adjustment measures to keep the particle flow stable.

Figure 7 shows the effect of the fluidizing number N_a on the pressure drop between the inlet and outlet of the air reactor. As

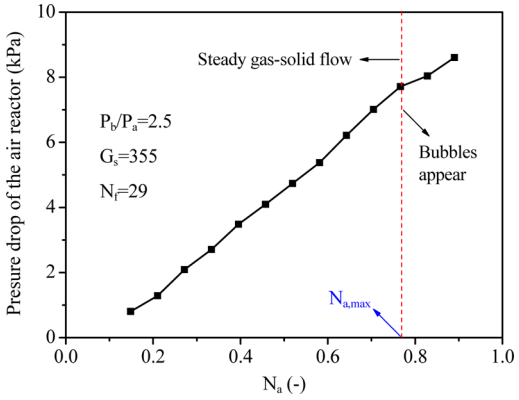

Figure 7. Effect of the fluidizing number, N_a, on the pressure drop of the moving bed.

expected, an increase in fluidizing number N_a results in a near-linear increase in the pressure drop of the air reactor before the value of N_a reaches the maximum (i.e., $N_{a,max}$) when the steady gas−solid flow starts to be broken. The average pressure drop is about 0.802 kPa for a fluidizing number N_a of 0.148 and increases to 7.71 kPa when N_a reaches $N_{a,max}$ (0.766). The relationship between the pressure drop and the fluidizing number N_a can be used to achieve the highest possible gas flow rate in the air reactor without disturbing the stable gas−solid flow.

Figure 8 presents the effect of solids mass flux G_s on the pressure drop between the inlet and outlet of the air reactor. It

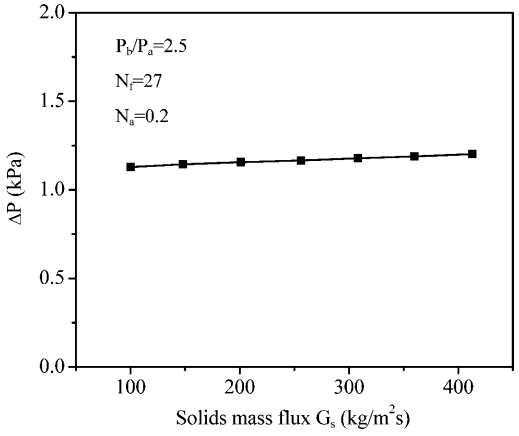

Figure 8. Effect of the solids mass flux, G_s, on the pressure drop of the moving bed.

DOI: 10.1021/acs.iecr.5b00471
Ind. Eng. Chem. Res. 2015, 54, 5749−5758

can be observed that the solids mass flux G_s has little impact on the pressure drop. With an increase in G_s from 100 to 413 kg/m^2·s, there was only a slight increase in the pressure drop of about 0.07 kPa. This indicates that a change in the solids mass flux has almost no effect on the gas−solid flow stability in the air reactor.

Figure 9 shows the effect of the pressure ratio P_b/P_a on the pressure drop of the air reactor. Considering that an increase in

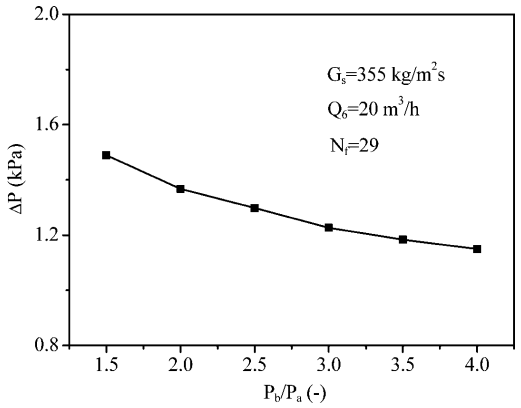

Figure 9. Effect of P_b/P_a on the pressure drop of the moving bed.

P_b/P_a might lead to part of the air bypassing into the first-stage inertial separator, hence making it hard to keep the fluidizing number N_a constant, we decided to keep the inlet superficial air flow rate of the moving bed Q_6, instead of N_a, constant during the investigation to reveal the effect of P_b/P_a on the pressure drop of the air reactor in a more rational and realistic way. It can be seen from Figure 9 that there was only a small decrease in the pressure drop of the air reactor (∼0.34 kPa) when P_b/P_a was increased from 1.5 to 4. However, a further increase in the pressure ratio to 5 was seen to lead to the generation of bubbles in the bed material layer above the air reactor. By that time, the system solids flux became unstable and kept decreasing, and finally, the solids circulation collapsed completely. Moreover, the advent of bubbles also indicated the bypassing of N_2 from the air reactor into the first-stage separator, which would lead to a reduction in CO_2 concentration. Therefore, adjustments of the pressure ratio P_b/P_a should be limited to a certain range that does not lead to the bypassing of N_2 from the air reactor into the first-stage separator.

The above results indicate that, during the operation of a practical CLC system, proper adjustments of the solids mass flux G_s or pressure ratio P_b/P_a will hardly affect the gas−solid flow stability in the air reactor. Thus, the fluidizing number N_a becomes the main influencing factor that can break the flow stability in the air reactor and, further, the whole system. Therefore, the relationship between the pressure drop and the fluidizing number N_a should be closely monitored in real time during system operation so as to pursue the highest possible inlet gas flow rate of the air reactor under the premise of stable gas−solid flows.

3.4. Separation Performance Experiment. *3.4.1. Selection of the Two-Stage Separators.* For an iG-CLC system with an HFCFB riser as the fuel reactor, it is difficult to achieve the complete conversion of char (also carbonaceous coal ash) just through a single loop in the riser because of the low reaction rate of gasification.[32] Thus, the conversion efficiency of carbon in coal will greatly depend on the recirculation efficiency of the separation system for the combustible particles (i.e., char and carbonaceous coal ash). In this respect, the novel iG-CLC system proposed in this study needs to achieve the following two targets: First, the first-stage separator should have a high separation efficiency for the large OC particles and a low separation efficiency for the fine combustible particles so as to prevent the latter from entering the air reactor and being consumed by air. Thus, it requires that the first-stage separator have a high selectivity for particle separation according to differences in the particle size and density. Second, the second-stage separator should have a high separation efficiency for fine particles so as to ensure that most of the combustible particles are circulated back to the fuel reactor.

To achieve these two requirements for the separation system, we designed an inertial separator as the first-stage separator, which was expected to be inefficient for separating fine coal particles but efficient enough for catching coarse OC particles. Meanwhile, we designed a cyclone as the second-stage separator, which was expected to be highly efficient for catching fine coal particles. Thus, the two-stage separation system was expected to achieve a high recirculation efficiency for the fine combustible particles. In addition, the combination of a low-resistance inertial separator and a high-resistance cyclone should be able to ensure a low pressure drop over the whole separation system under high-flux conditions.

3.4.2. Separation Efficiencies. A series of separation performance tests was conducted to confirm whether the two-stage separation system had both a high global separation efficiency (i.e., η) and a selective separation efficiency (i.e., η_s) for fine particles, which are required to achieve a high conversion of carbon in coal.

Table 3 presents some important parameters measured during the separation performance tests. The relevant

Table 3. Measurement Parameters of the Separation Performance Tests

description	value
output solids mass rate of the first-stage downcomer, M_0 (kg/h)	1021
mass fraction of coal in the output solids flow of the first-stage downcomer, Y_0	4.41×10^{-2}
mass flow rate of solids separated by the second-stage separator, M_2 (kg/h)	35
mass fraction of coal in the solid particles separated by the second-stage separator, Y_2	∼1
mass flow rate of solids separated by the first-stage separator, M_1 (kg/h)	986
testing time t (s)	300
mass of solids collected by the bag filter during the testing time, $m_3(t)$ (kg)	∼0.02

experimental procedure and data evaluation can be found in sections 2.3.4 and 2.4.5, respectively. Figure 10 shows the derived values of the global separation efficiency η and the selective separation efficiency η_s of the two-stage separation system for fine coal particles. It can be seen that the global separation efficiency η reached about 99.5% under the operating conditions of G_s = 100 kg/m^2·s and N_f = 33, indicating that a very high capture efficiency of the two-stage separation system for fine combustible particles is achievable with a practical iG-CLC system. The value of the selective separation efficiency η_s reached about 77.7%, indicating the achievement of a relatively high selectivity of the two-stage separation system for fine particles. Thus, a large proportion of

DOI: 10.1021/acs.iecr.5b00471
Ind. Eng. Chem. Res. 2015, 54, 5749−5758

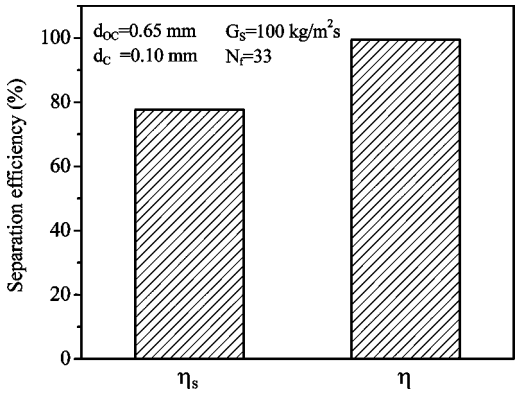

Figure 10. Global separation efficiency, η, and selective separation efficiency, η_s, of the two-stage separation system for fine coal particles.

fine combustible particles will escape from the first-stage inertial separator and then be separated by the second-stage cyclone separator into the fuel reactor for further reaction. In future iG-CLC applications, the selective separation efficiency η_s can be further enhanced by properly reducing the baffle height of the first-stage inertial separator or selecting coal particles with smaller sizes. Therefore, we conclude that the designed two-stage separation system can achieve the objective of separating most of the fine combustible particles back to the fuel reactor for further reaction so as to ensure a high carbon conversion.

4. CONCLUSIONS

This study presents an improved cold experimental system for a novel iG-CLC system consisting of an HFCFB riser as the fuel reactor, a cross-flow moving bed as the air reactor, and a two-stage separation system. Through a series of experimental investigations on this improved cold iG-CLC system, we achieved almost all of the initial goals set for the improved cold experimental system that will guide our future testing program with a hot experimental system:

(1) The implementation of steady operations by adjusting system parameters provides valuable experience for the debugging of the future hot system.
(2) Achieving higher solids fluxes (>400 kg/m^2·s) and solids holdups (>0.05) in the CFB riser can enhance gas−solid contact and reaction in the fuel reactor.
(3) The increased carrying capacity of the gas flow in the improved air reactor ($N_{a,max}$ increased from 0.132 to 0.766) greatly reduces the requirement for the cross-sectional area of the air reactor and, hence, can lead to an increase in the power capacity of the overall iG-CLC system.
(4) The ability to control the gas flow directions in the two reactors (f_{II} = 0, f_I = 0.23%) means that the gas bypassing between the two reactors can be restrained so as to keep a high CO_2 concentration in the exhaust of the fuel reactor and a high capture efficiency of CO_2.
(5) The high selective separation efficiency (77.7%) and global separation efficiency (99.5%) of the new two-stage separation system for fine particles can ensure a high combustion efficiency of coal with a hot iG-CLC system.

AUTHOR INFORMATION

Corresponding Authors

*Tel.: +86-25-83794744. Fax: +86-25-83795508. E-mail: bsjin@seu.edu.cn.
*Tel.: +44-115-8467674. Fax: +44-115-9513159. E-mail: liu.hao@nottingham.ac.uk.

Notes

The authors declare no competing financial interest.

ACKNOWLEDGMENTS

The financial support of the reported research by the National Natural Science Foundation of China (51076029), the UK Engineering and Physical Sciences Research Council (EPSRC/China Project EP/G063176/1), the Ministry of Science and Technology of China (China-EU International Collaboration Project 2010DFA61960), the Scientific Research Foundation of Graduate School of Southeast University (YBPY1401, YBJJ1119), and China Academic Award for Doctoral Candidates is gratefully acknowledged. The authors also acknowledge the provision of a scholarship to X.W. by the China Scholarship Council (CSC) that enabled him to carry out part of the reported work at the University of Nottingham.

NOMENCLATURE

f_I = fraction of the fuel reactor flue gas passing into the air reactor
f_{II} = fraction of gas from the air reactor inlet passing into the second-stage cyclone outlet
G_s = solids mass flux, kg m^{-2} s^{-1}
M_0 = output solids mass flow rate (including OC and coal), kg h^{-1}
M_1 = mass flow rate of solids separated by the first-stage separator, kg h^{-1}
M_2 = mass flow rate of solids separated by the second-stage separator, kg h^{-1}
M_3 = mass flow rate of solids separated by the bag filter, kg h^{-1}
$m_3(t)$ = mass of solids collected by the bag filter during the testing time, kg
N_a = fluidizing number in the air reactor
$N_{a,max}$ = maximum fluidizing number in the air reactor
N_f = fluidizing number in the fuel reactor
P = pressure, kPa
ΔP_Z = local pressure drop at two adjacent riser elevations, kPa
$Q_{1,sta}$ = inlet air flow rate of the riser, m^3 h^{-1}
$Q_{2,sta}$ = fluidizing air flow rate of the first-stage J valve, m^3 h^{-1}
$Q_{3,sta}$ = aeration air flow rate of the first-stage J valve, m^3 h^{-1}
$Q_{4,sta}$ = aeration air flow rate of the second-stage J valve, m^3 h^{-1}
$Q_{5,sta}$ = aeration air flow rate of the feeder, m^3 h^{-1}
$Q_{6,sta}$ = inlet air flow rate of the moving bed, m^3 h^{-1}
$Q_{a,sta}$ = outlet flow rate of the second-stage cyclone separator, m^3 h^{-1}
$Q_{b,sta}$ = outlet air flow rate of the moving bed, m^3 h^{-1}
$Q_{g,sta}$ = sum of $Q_{1,sta}$−$Q_{5,sta}$, m^3 h^{-1}
$Q_{in,sta}$ = total inlet flow rate of the system, m^3 h^{-1}
$Q_{out,sta}$ = total outlet flow rate of the system, m^3 h^{-1}
t = testing time of the separation performance experiment, s
U_a = superficial gas velocity of the air reactor, m^3 s^{-1}
U_f = superficial gas velocity of the fuel reactor, m s^{-1}

DOI: 10.1021/acs.iecr.5b00471
Ind. Eng. Chem. Res. 2015, 54, 5749−5758

U_{min} = minimum fluidization gas velocity of the bed material, m s^{-1}
$x_{a,CO}$ = concentration of tracer gas I at the outlet of the second-stage cyclone separator, ppm
$x_{b,CO}$ = concentration of tracer gas I at the outlet of the moving bed, ppm
$x'_{a,CO}$ = concentration of tracer gas II at the outlet of the second-stage cyclone separator, ppm
$x'_{b,CO}$ = concentration of tracer gas II at the outlet of the moving bed, ppm
Y_0 = initial mass fraction of coal in the solid particles in the first-stage downcomer
Y_1 = mass fraction of coal in the solid particles separated by the first-stage separator
Y_2 = mass fraction of coal in the solid particles separated by the second-stage separator
Y_3 = mass fraction of coal in the solid particles separated by the bag filter
ΔZ = height difference between two adjacent riser elevations, m

Greek Letters

ε_s = apparent cross-sectional average solids holdup
η = global separation efficiency of the two-stage separation system for fine coal particles
η_s = selective separation efficiency of the two-stage separation system for fine coal particles
ρ_g = air density, kg m^{-3}
ρ_s = density of bed material, kg m^{-3}

REFERENCES

(1) Fan, L. S. *Chemical Looping Systems for Fossil Energy Conversions*; Wiley-AIChE: New York, 2010.
(2) Lyngfelt, A.; Leckner, B.; Mattisson, T. A fluidized-bed combustion process with inherent CO_2 separation; application of chemical-looping combustion. *Chem. Eng. Sci.* **2001**, *56*, 3101.
(3) Mattisson, T.; García-Labiano, F.; Kronberger, B.; Lyngfelt, A.; Adánez, J.; Hofbauer, H. Chemical-looping combustion using syngas as fuel. *Int. J. Greenhouse Gas Control* **2007**, *1*, 158.
(4) Abad, A.; Mattisson, T.; Lyngfelt, A.; Johansson, M. The use of iron oxide as oxygen carrier in a chemical-looping reactor. *Fuel* **2007**, *86*, 1021.
(5) Forero, C. R.; Gayán, P.; de Diego, L. F.; Abad, A.; García-Labiano, F.; Adánez, J. Syngas combustion in a 500 W_{th} chemical-looping combustion system using an impregnated Cu-based oxygen carrier. *Fuel Process. Technol.* **2009**, *90*, 1471.
(6) Cao, Y.; Pan, W. P. Investigation of chemical looping combustion by solid fuels. 1. Process analysis. *Energy Fuels* **2006**, *20*, 1836.
(7) Berguerand, N.; Lyngfelt, A. Design and operation of a 10 kW_{th} chemical-looping combustor for solid fuels—Testing with South African coal. *Fuel* **2008**, *87*, 2713.
(8) Leion, H.; Mattisson, T.; Lyngfelt, A. Solid fuels in chemical-looping combustion. *Int. J. Greenhouse Gas Control* **2008**, *2*, 180.
(9) Shen, L. H.; Wu, J. H.; Xiao, J. Experiments on chemical looping combustion of coal with a NiO based oxygen carrier. *Combust. Flame* **2009**, *156*, 721.
(10) Xiao, R.; Song, Q. L.; Song, M.; Lu, Z. J.; Zhang, S.; Shen, L. H. Pressurized chemical-looping combustion of coal with an iron ore-based oxygen carrier. *Combust. Flame* **2010**, *157*, 1140.
(11) Abad, A.; Gayán, P.; de Diego, L. F.; García-Labiano, F.; Adánez, J. Fuel reactor modelling in chemical-looping combustion of coal: 1. Model formulation. *Chem. Eng. Sci.* **2013**, *87*, 277.
(12) García-Labiano, F.; de Diego, L. F.; Gayán, P.; Abad, A.; Adánez, J. Fuel reactor modelling in chemical-looping combustion of coal: 2. Simulation and optimization. *Chem. Eng. Sci.* **2013**, *87*, 173.
(13) Cuadrat, A.; Abad, A.; Gayán, P.; de Diego, L. F.; García-Labiano, F.; Adánez, J. Theoretical approach on the CLC performance with solid fuels: Optimizing the solids inventory. *Fuel* **2012**, *97*, 536.
(14) Wang, X. J.; Jin, B. S.; Zhang, Y.; Zhang, Y.; Liu, X. L. Three Dimensional Modeling of a Coal-Fired Chemical Looping Combustion Process in the Circulating Fluidized Bed Fuel Reactor. *Energy Fuels* **2013**, *27* (4), 2173.
(15) Wang, X. J.; Jin, B. S.; Liu, X. L.; Zhang, Y.; Liu, H. Experimental Investigation on Flow Behaviors in a Novel in Situ Gasification Chemical Looping Combustion Apparatus. *Ind. Eng. Chem. Res.* **2013**, *52*, 14208.
(16) Abad, A.; Adánez, J.; Cuadrat, A.; García-Labiano, F.; Gayán, P.; de Diego, L. F. Kinetics of redox reactions of ilmenite for chemical-looping combustion. *Chem. Eng. Sci.* **2011**, *66*, 689.
(17) Adánez, J.; Cuadrat, A.; Abad, A.; Gayán, P.; de Diego, L. F.; García-Labiano, F. Ilmenite activation during consecutive redox cycles in chemical-looping combustion. *Energy Fuels* **2010**, *24*, 1402.
(18) Cuadrat, A.; Abad, A.; Adánez, J.; de Diego, L. F.; García-Labiano, F.; Gayán, P. Behavior of ilmenite as oxygen carrier in chemical-looping combustion. *Fuel Process. Technol.* **2012**, *94*, 101.
(19) Cuadrat, A.; Abad, A.; García-Labiano, F.; Gayán, P.; de Diego, L. F.; Adánez, J. Effect of operating conditions in chemical-looping combustion of coal in a 500 W_{th} unit. *Int. J. Greenhouse Gas Control* **2012**, *6*, 153.
(20) Bischi, A.; Langørgen, Ø.; Saanum, I.; Bakken, J.; Seljeskog, M.; Bysveen, M.; Morin, J.-X.; Bolland, O. Design study of a 150 kW_{th} double loop circulating fluidized bed reactor system for chemical looping combustion with focus on industrial applicability and pressurization. *Int. J. Greenhouse Gas Control* **2011**, *5*, 467.
(21) Kolbitsch, P.; Pröll, T.; Hofbauer, H. Modeling of a 120 kW chemical looping combustion reactor system using a Ni-based oxygen carrier. *Chem. Eng. Sci.* **2009**, *64*, 99.
(22) Markström, P.; Lyngfelt, A.; Linderholm, C. Chemical-looping combustion in a 100 kW unit for solid fuels. Presented at the *21st International Conference on Fluidized Bed Combustion*, Naples, Italy, Jun 3–6, 2012.
(23) Ströhle, J.; Orth, M.; Epple, B. Design and operation of a 1 MWth chemical looping plant. *Appl. Energy* **2014**, *113*, 1490.
(24) Ströhle, J.; Lombarte, A.; Orth, M.; Epple, B. Simulation of a chemical looping combustion process for coal. Presented at the *1st International Oxyfuel Combustion Conference*, Cottbus, Germany, 2009.
(25) Hsiau, S. S.; Smid, J.; Tsai, F. H.; Kuo, J. T.; Chou, C. S. Velocities in moving granular bed filters. *Powder Technol.* **2001**, *114*, 205.
(26) Smid, J.; Hsiau, S. S.; Tsai, S. A.; Tzeng, C. C.; Chyou, Y. P. Study on gravity flow of granules in beds supported by louver–sublouver system. *Adv. Powder Technol.* **2009**, *20*, 127.
(27) Chen, Y. H.; Zhu, X. D.; Wu, Y. Q.; Zhu, Z. B. Investigation of the Effect of a Dividing Wall in a Moving Bed. *Chem. Eng. Technol.* **2007**, *30*, 1028.
(28) Wang, X. F.; Jin, B. S.; Zhong, W. Q. Flow Behaviors in a High-Flux Circulating Fluidized Bed. *Int. J. Chem. React. Eng.* **2008**, 6.
(29) Issangya, A. S.; Bai, D.; Bi, H. T.; Lim, K. S.; Zhu, J.; Grace, J. R. Suspension densities in a high-density circulating fluidized bed riser. *Chem. Eng. Sci.* **1999**, *54*, 5451.
(30) Namkung, W.; Kim, S. W.; Kim, S. D. Flow regimes and axial pressure profiles in a circulating fluidized bed. *Chem. Eng. J.* **1999**, *54*, 245.
(31) Li, Z. Q.; Wu, C. N.; Wei, F.; Jin, Y. Experimental study of high-density gas–solids flow in a new coupled circulating fluidized bed. *Powder Technol.* **2004**, *139*, 214.
(32) Xiao, R.; Chen, L.; Saha, C.; Zhang, S.; Bhattacharya, S. Pressurized chemical-looping combustion of coal using an iron ore as oxygen carrier in a pilot-scale unit. *Int. J. Greenhouse Gas Control* **2012**, *10*, 363–373.

DOI: 10.1021/acs.iecr.5b00471
Ind. Eng. Chem. Res. 2015, 54, 5749–5758